Polymer-mediated drug supersaturation - a spotlight on the interplay between phase-separated amorphous drug colloids and dissolved molecules

Ozan Hirlak[1], Sabine Dieluweit[2], Rudolf Merkel[2], Karl G. Wagner[1]*

[1]*Department of Pharmaceutical Technology and Biopharmaceutics, University of Bonn, 53121 Bonn, Germany*

[2]*Institute of Biological Information Processing: IBI-2, Forschungszentrum Jülich, 52425 Jülich, Germany*

*Corresponding author.
Contact:
Karl G. Wagner
Department of Pharmaceutical Technology and Biopharmaceutics, University of Bonn, Gerhard-Domagk-Str. 3, 53121 Bonn, Germany
E-Mail: karl.wagner@uni-bonn.de
Tel.: +49 228 735271, Fax: +49 228 735268

Abstract

Hypothesis

Colloidal aggregation phenomena have been found responsible for the supersaturation of poorly water-soluble drugs, potentially leading to bioavailability enhancements. Unlike coarse precipitates, phase separation in the form of colloids, is expected to enhance drug supersaturation performance. Therefore, a high proportion of these colloids should correlate with the extent and the kinetics of supersaturation. The prime objective of the current study is to provide a mechanistic understanding on supersaturation for the model drug albendazole (ALB) in combination with twelve polymers.

Experiments

Species separated after a pH-shift were characterized by dynamic light scattering (DLS), freeze-fracture electron microscopy (FF-EM) and transmission X-ray diffraction (XRD). Laser diffraction (LD) in a liquid cell was introduced for a relative quantification of the colloidally separated species, described as colloid fraction. The pH-dependent supersaturation was assessed online using a miniaturized dissolution assay.

Findings

Here, a measure of the extent of amorphous colloidal phase separation was established, and its impact on supersaturation was evaluated. As a result, a correlation was found between the extent of supersaturation and the colloid fraction. This confirmed the dependence of polymer-mediated enabling and preservation of supersaturation on the ability of polymers to stabilize colloid fractions. Furthermore, a fixed ratio was suggested between the dissolved drug and colloidally separated drug as the kinetic profiles of both species showed similar trajectories. In conclusion, colloid fractions were identified to be responsible for dissolved and potentially bioavailable drug molecules.

Keywords

Supersaturation, Amorphous colloidal phase separation, Kinetics, Colloid, Precipitation, Recrystallization, Solid-state, Freeze-fracture electron microscopy, Particle size distribution

1 Introduction

The biopharmaceutics classification system (BCS) classifies orally administered drugs according to their aqueous solubility and membrane permeability (Amidon et al., 1995). Despite their high permeability, BCS class II drugs suffer from a reduced bioavailability due to their poor aqueous solubility at the absorption site as mainly dissolved molecules can be absorbed. Pharmaceutical formulations and

excipients that increase the bioavailability of these drugs are characterized by drug supersaturation in *in vitro* test systems (Fong et al., 2017; Kohri et al., 1999). Within this context, the "spring" effect generates an increase of the drug concentration above its equilibrium solubility, and the "parachute" effect, on the other hand, stabilizes the drug concentration at the supersaturated level (Guzmán et al., 2007).

Upon the supersaturation of poorly water-soluble drugs, amorphous colloidal phase separation, e.g. liquid-liquid phase separation, potentially occurs, where nano-sized amorphous drug species disperse within the continuous aqueous phase (França et al., 2020; Ganesh et al., 2018; Indulkar et al., 2016; Kawakami, 2017; Laitinen et al., 2017). Phase separation and supersaturation of weakly basic drugs have been previously observed by Indulkar et al., 2015 upon pH shift. The amorphous colloidal drug phase not only serves as a reservoir for dissolved drug molecules, but also potentially boosts their oral bioavailability (Indulkar et al., 2016; Kesisoglou et al., 2019; Stewart et al., 2017; Wilson et al., 2018). Consequently, the existence of three drug species in parallel can be assumed: a) molecularly dissolved drug fraction, b) phase-separated amorphous drug colloids and c) drug precipitated as solid particles, either amorphous or crystalline (Indulkar et al., 2016; Morrison et al., 2017; Raina et al., 2015; Van Eerdenbrugh et al., 2014). Adjunct to the molecularly dissolved drug, amorphous colloids should have higher impact on the supersaturation performance and bioavailability enhancement compared to particulate matter of amorphous or even crystalline solid-state.

In this paper, an investigation on how phase separation phenomena and supersaturation phenomena induced by a pH shift correlate with each other for the BCS class II model drug albendazole (ALB) was conducted. The expected phase separation and precipitation behavior induced by a pH shift is shown in Fig. 1. ALB represents a weakly basic drug (pKa = 2.8), which is highly soluble at low pH values present in the stomach, but practically insoluble at higher pH values present at the absorption site (Surasarang et al., 2017). Therefore, a rapid precipitation was expected for neat ALB in the applied supersaturation assay shifting the pH from 1 to 5.5 due to a conversion of the protonated molecule to the free base. We assumed that an amorphous colloidal phase separation phenomenon occurring prior to precipitation can significantly determine the extent and kinetics of supersaturation. Hence, it is expected that polymers that can enable and preserve supersaturation stabilize the amorphous nano-sized drug species that are forced to separate from the solution by the pH shift to create the above mentioned second phase. As a consequence, a correlation between the extent of amorphous colloidal phase separation and the supersaturation is expected. However, quantitative relations between the extent of the former and the latter have not yet been established. Here, we introduce an at-line particle-size measurement method based on laser diffraction (LD) to quantify the relative proportions of colloidally separated ALB within the total precipitate, henceforth referred to as "colloid fraction". This might serve as a descriptor for the supersaturation kinetics. This method represents a novel tool to evaluate the performance of supersaturating systems designed to increase the drug bioavailability. The amorphous colloidal phase separation was confirmed using dynamic light scattering (DLS), freeze-fracture electron microscopy (FF-EM) and transmission X-ray diffraction (XRD). Based on the findings, this paper might provide an improved understanding of the phenomena underlying drug supersaturation.

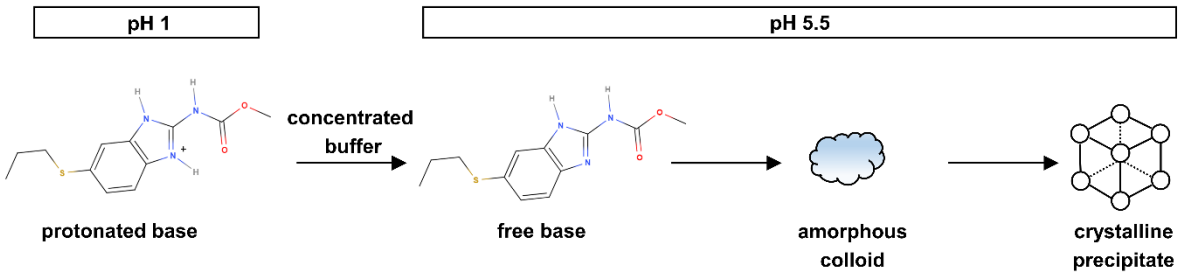

Fig. 1. Expected precipitation and phase separation behavior of neat ALB in dependence of pH. A conversion of the protonated base to the free base leads to rapid recrystallization. The amorphous colloids represent a separated phase, which might influence kinetics and extent of supersaturation.

2 Materials and Methods

2.1 Materials

ALB was purchased from Sigma-Aldrich (Steinheim, Germany). Methylcellulose (MC A4C) was obtained from Colorcon (Kent, UK). The average molecular weight (av. *M*r) of MC A4C is 212 kDa. The hydroxypropyl methylcellulose (HPMC) grades HPMC 15LV (av. *M*r = 84 kDa), HPMC 100LV (av. *M*r = 170 kDa) and HPMC 4M (av. *M*r = 550 kDa) were obtained from DuPont (Wilmington, Delaware, USA). Copovidon (COP) (polyvinylpyrrolidone–vinyl acetate copolymer, av. *M*r = 58 kDa) as well as the three polyvinylpyrrolidone (PVP) grades PVP K-10 (av. *M*r = 3 kDa), PVP K-30 (av. *M*r = 49 kDa) and PVP K-90 (av. *M*r = 1750 kDa) were donated by BASF (Ludwigshafen, Germany). The hydroxypropyl cellulose (HPC) grades HPC SL (av. *M*r = 100 kDa) and HPC SSL (av. = *M*r 40 kDa) were provided by Nisso Chemical Europe (Düsseldorf, Germany). Different grades of the polyethylene glycol (PEG) including PEG 6k (av. *M*r = 6 kDa) and PEG 10k (av. *M*r = 10 kDa) were purchased from Carl Roth (Karlsruhe, Germany). Sodium chloride, sodium hydroxide, ammonium dihydrogen phosphate and methanol were purchased from VWR Chemicals (Darmstadt, Germany). Tri-potassium phosphate and tri-potassium citrate were obtained from Alfa Aesar (Kandel, Germany) and Carl Roth (Karlsruhe, Germany), respectively. All polymers were of pharmaceutical grade, and all other chemicals were of analytical grade.

2.2 Methods

2.2.1 Saturation solubility

Saturation solubility of ALB was determined in 0.1 M hydrochloric acid (HCl) (pH 1.0) and phosphate buffer (pH 5.5). Additionally, the impact of dissolved polymers on the saturation solubility was assessed in phosphate buffer (pH 5.5) at a respective polymer level of 0.4 mg/mL. The samples were shaken in a water bath at 37 °C for 24 hours. Before analysis, the samples were filtered through 0.22 µm polyethersulfone filters. 20 µL of the filtrate was injected into an Agilent 1100 high performance liquid chromatography separations module (Agilent Technologies GmbH, Waldbronn, Germany) equipped with a reversed-phase C18 column. The samples were eluted with a mobile phase consisting of 30% ammonium dihydrogen phosphate buffer (1.67 g/L) and 70% methanol at 1 mL/min flow rate. Peaks were detected at a wavelength of 210 nm using a photodiode array detector (Agilent G1315B).

2.2.2 Dynamic light scattering (DLS)

The initial particle size of colloidally separated ALB was investigated by means of DLS, a method used for the detection of separated drug colloids (Ganesh et al., 2018; Taylor and Zhang, 2016). A clear sample solution of 2 mL with an ALB concentration of 0.1 mg/mL and an excipient concentration of 0.4 mg/mL in 0.1 M HCl was mixed with a magnetic stirrer in a water bath at 37 °C. A concentrated buffer consisting of 0.375 M phosphate buffer and 0.85 M sodium hydroxide was prepared for pH adjustments (Monschke and Wagner, 2019). After the addition of 0.162 mL of the concentrated buffer

to the sample solution, the pH increased to 5.5, which induced precipitation. One minute after the pH shift, the obtained samples were transferred into a quartz glass cuvette for subsequent analysis in the SZ-100 Nanoparticle Analyzer (Horiba, Kyoto, Japan) at a 90° side scatter detector angle. The light source was a green laser diode with a wavelength of 532 nm operating at 10 mW. For each sample, the hydrodynamic diameter expressed as Z-average as well as the polydispersity index (PDI) were reported by the manufacturer´s software (Horiba SZ-100 for Windows software version 1.90). The mean values and standard deviations were based on the measurements of three individual samples.

2.2.3 Laser diffraction (LD)

The volume-based particle size distributions and the relative fractions in a predetermined particle size range of both precipitated and colloidally separated ALB species were measured with a Horiba LA-960 laser diffractometer (Horiba, Kyoto, Japan) over time. A red laser diode with 650 nm wavelength (5 mW) and a blue light emitting diode (3 mW) with 405 nm wavelength were used as light sources. The volume of the clear sample solution described in 2.2.2 was increased to 15 ml while maintaining the corresponding concentrations of the drug and excipient. This clear sample solution was mixed in a water bath at 37 °C for 30 min. Subsequently, the pH shift was introduced by adding 1.215 ml of the concentrated buffer to the clear sample solution to increase the pH to 5.5. The total volume of the obtained samples was transferred in quartz glass cuvette at predetermined points in time for at-line measurements (31, 35, 40, 50, 60 and 90 min; i.e. 1, 5, 10, 20, 30 and 60 min after the pH shift). A magnetic stirrer was placed in the cuvette in order to agitate the sample. After each measurement, the sample solutions were transferred back into the water bath. The experiments were conducted in triplicate resulting in three size distributions from three individual measurements, which were used to calculate mean values and standard deviations.

2.2.4 Supersaturation assay

The supersaturation performance of ALB was tested in the MiniDissolution apparatus (Zecevic and Wagner, 2013) using a pH-shift method at 37 °C with a paddle speed of 75 rpm. Initially, the drug and the respective excipient were pre-dissolved in 20 ml 0.1 M HCl at concentrations of 100 µg/mL and 400 µg/mL, respectively. This resulted in the same drug and excipient concentrations as described under the sections 2.2.2 and 2.2.3. After 30 min, the pH of the dissolution medium was adjusted to 5.5 by adding 1.62 mL of the concentrated buffer. The assay was then continued at this pH stage for another 60 min. The absorption spectra were collected online at predetermined points in time (every 5 min for the first 30 min; every 3 min for the next 30 min; every 5 min for the last 30 min) using a diode array UV/VIS spectrophotometer (Agilent 8453, Agilent Technologies GmbH, Waldbronn, Germany). Drug concentrations were determined by derivation of the absorption spectra in order to correct UV/VIS baseline shifts due to light scattering effects.

2.2.5 X-ray diffraction (XRD)

The solid-state of ALB species was examined with $CuK\alpha_1$ radiation generated at 45 kV and 40 mA over the 2θ range of 10° to 30° in increments of 0.04°/min using the X'Pert MRD Pro diffractometer (PANalytical B.V., Almelo, Netherlands) in the transmission mode. Samples adjusted to pH 5.5 at 37 °C were centrifuged at 21380 *g* while maintaining this temperature constant. After removal of the supernatant, the wet sample was measured six consecutive times, with one measurement requiring approximately 10 min.

2.2.6 Freeze-fracture scanning electron microscopy (FF-EM)

1 µl was drawn from the samples described under section 2.2.2 after the pH-shift. The freeze-fracturing was performed following the procedure based on Moor and Mühlethaler, 1963 and Severs, 2007. The aliquots were quickly frozen in liquid ethane, cooled down by liquid nitrogen. Subsequently, the frozen samples were inserted in a freeze etching apparatus BAF 400T (Balzers, Lichtenstein, now: Leica

Microsystems). Cutting and etching were performed in the temperature range of -114 °C to -117 °C. Evaporation of platinum and carbon at 45° was followed by the evaporation of carbon at 90° on rotating samples, which resulted in a replica. The replica (Pt/C layer thickness of around 2 nm and C layer thickness in the range between 20 - 30 nm) was separated from the sample by floating on dimethyl sulfoxide and water solution followed by a transfer on electron microscopy copper grids (Athene old, Plano, Wetzlar, Germany). The samples were then analyzed by scanning transmission electron microscopy (STEM), applying 25 kV acceleration voltage at 0.1 nA in bright field mode using a Magellan 400 electron microscope (Albrecht et al., 2017) (FEI, Hillsboro, Oregon, USA).

3 Results

3.1 Saturation solubility

The saturation solubility of the protonated ALB base was 2.25 ± 0.01 mg/mL at pH 1. In contrast, only 2.41 ± 0.26 µg/mL of the drug was dissolved at pH 5.5, indicating the poor aqueous solubility of the free ALB base (Fig. 2). Among all excipients tested, only the hydroxypropyl methylcellulose (HPMC) grades and copovidone (COP) significantly increased the saturation solubility of ALB. The highest solubility enhancement was observed in the presence of HPMC 100LV, where a saturation solubility of 3.35 ± 0.35 µg/mL was obtained. In contrast the hydroxypropyl cellulose (HPC), polyvinylpyrrolidone (PVP), polyethylene glycol (PEG) grades and methyl cellulose (MC) A4C showed no significant effect on the saturation solubility of ALB.

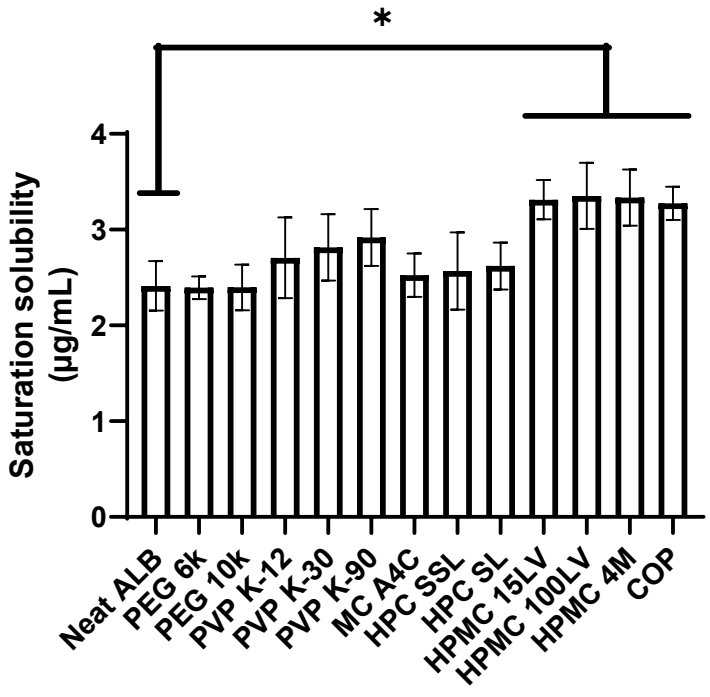

Fig. 2. Saturation solubility of ALB in presence and absence of excipients at pH 5.5. The star (*) highlights a statistically significant difference between the samples derived from a one-way ANOVA test (p-value < 0.05). Error bars represent the standard deviations of the values. The experiments were conducted in triplicate.

3.2 DLS measurements 1 min after pH shift

At pH 1 the ALB solution is clear due to the high drug solubility at this pH stage. A pH shift to pH 5.5 induced precipitation, but also potential supersaturation as the solubility of the drug decreased dramatically. In order to detect colloidal phase separation, the samples were characterized using DLS. Within the first minute after the pH-shift, ALB showed colloidal phase separation both in the presence and absence of the excipients, as the colloid size was in the nanometer range (Table 1). As a result, the solutions appeared slightly bluish albeit still transparent. The Z-average of ALB colloids was 251 ± 15 nm. In the presence of HPMC 100LV and MC A4C, the Z-average was 228 ± 23 nm and 224 ± 16 nm, respectively. PDI values between 0.33 ± 0.07 and 0.82 ± 0.14 indicate polydisperse particle size distributions.

Table 1. Z-average and polydispersity index (PDI) values of ALB colloids separated in presence and absence of excipients are shown. Neat ALB as well as all ALB-polymer combinations formed a separated phase immediately after the shift from pH 1 to pH 5.5. High PDI values indicate polydisperse particle size distributions. Results are presented as mean value ± standard deviation. The experiments were conducted in triplicate.

	Z-Average (nm)	PDI
Neat ALB	251 ± 15	0.54 ± 0.21
PEG 6k	262 ± 52	0.45 ± 0.26
PEG 10k	270 ± 71	0.82 ± 0.14
PVP K-12	190 ± 85	0.39 ± 0.13
PVP K-30	168 ± 32	0.34 ± 0.08
PVP K-90	180 ± 11	0.70 ± 0.05
MC A4C	224 ± 16	0.67 ± 0.28
HPC SSL	167 ± 19	0.51 ± 0.22
HPC SL	163 ± 17	0.34 ± 0.23
HPMC 15LV	267 ± 29	0.36 ± 0.14
HPMC 100LV	228 ± 23	0.48 ± 0.34
HPMC 4M	265 ± 21	0.69 ± 0.37
COP	177 ± 10	0.33 ± 0.07

3.3 Time-dependent particle size distributions of the separated phase

The slightly bluish and at the same time transparent appearance of the ALB solutions rebuffered to pH 5.5 was only observed for a short period of time. The rebuffered solution was analyzed by LD at predetermined points in time to monitor the development of the particle size distributions of ALB species over time. The particle size distributions obtained 1, 30 and 60 min after the pH shift are shown in Fig. 3, Sup. 1 and Sup. 2. In the first minute after the pH shift, a bimodal particle size distribution was observed for neat ALB. The majority of the separated ALB species were found in the colloidal size range below 1 µm. These species were responsible for the slightly blue appearance of the sample, as they scatter the light. The cumulative distribution curve shows that 90.2 ± 5.4% of the species were smaller than 1 µm (data not shown). On the contrary, a lower proportion of the ALB species recrystallized in the range between 1 µm and 10 µm. Henceforth, the relative volume-based proportion of ALB

separated below 1 µm is defined as the colloid fraction. In contrast, the relative volume-based proportion of ALB separated above 1 µm is defined as the coarse fraction. 5 min after the pH shift, the colloid fraction already decreased dramatically (data not shown). As a result, the main proportion of the species was found in the size range between 1 and 100 µm. 30 and 60 min after the pH shift, the colloid fraction dropped to an even lower level. Furthermore, the species in the coarse fraction appeared to agglomerate, as indicated by the formation of a peak between 100 and 1000 µm. The addition of each tested excipient resulted in bimodal particle size distributions of the separated ALB species over the entire period of the measurements. However, the time-dependent development of the colloid fraction within the separated phase was specifically influenced by the type of the added excipient. Considering the particle size distributions from Fig. 3, it is evident that the colloid fraction decreased over time in the presence of MC A4C, but was yet much more pronounced compared to neat ALB. In the presence of HPMC 100LV, the colloid fraction was even higher than in the presence of MC A4C, emphasizing the high colloid stabilization potential of the polymers used. Since the results were based on relative volume-based distributions, the coarse fractions always behaved in the opposite manner to the colloid fractions.

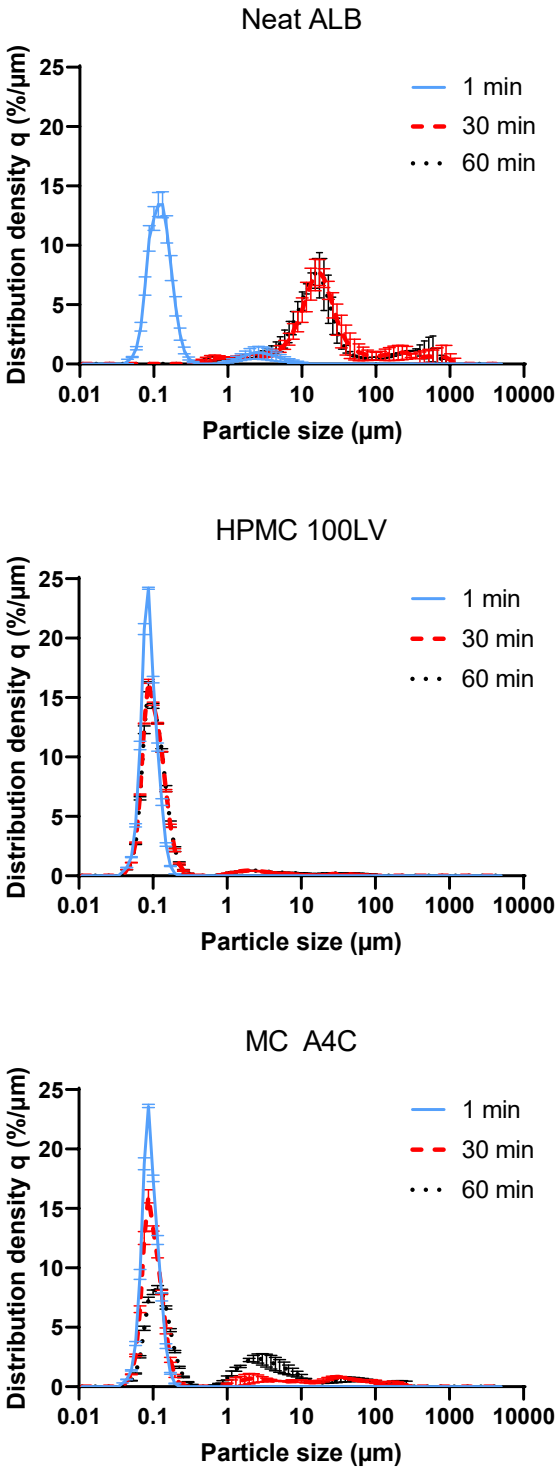

240

Fig. 3. Volume-based particle size distributions of ALB species measured by means of laser diffraction in absence of polymers and in combination with HPMC 100LV and MC A4C, respectively. The blue solid line, the red dashed line and the black dotted line were obtained 1 min, 30 min and 60 min after the shift from pH 1 to pH 5.5 respectively. Bimodal distributions indicate that a colloid fraction and a
245 coarse fraction were formed after the pH shift. Peak heights changed over time depending on the type of the polymer added. Error bars represent the standard deviations of the values. The experiments were conducted in triplicate.

3.4 Kinetic profiles of the colloid fractions

The kinetic profiles of the colloid fractions shown as red lines in Fig. 4, Sup. 3 and Sup. 4 were created from the particle size distributions obtained by LD, in order to illustrate their time-dependent evolution. For this purpose, the relative proportion of species smaller than 1 µm was used as a cut-off point, which can be derived from the cumulative particle size distribution curve. The cut-off point corresponded to the area under the curve (AUC) of the volume-based particle size distribution curve (section 3.3) normalized to equal distances at the x-axis, which was located in the submicron range. Using the quantification method mentioned previously, the colloid fraction, which described the relative proportion of species smaller than 1 µm within the separated phase, was determined. Then, the cut-off point was plotted against the measurement times, whereby the colloid fraction profile was obtained.

Within the first 30 min at pH 1, neither did the colloidal ALB species separate nor did a precipitate form as the drug was present only in a molecularly dissolved state resulting in clear sample solutions. From this, it follows that the colloid fraction profiles were zero in the first 30 min (before the pH shift was conducted) for all measurements. Immediately after pH shift from 1.0 to 5.5, a colloid fraction was formed for all samples. However, the various colloid fractions varied strongly in their kinetic stability. For neat ALB, the colloid fraction 1 min after the pH shift was 90.2 ± 5.4% followed by an exponential decay leaving only 5.8 ± 1.2% 9 min later. In contrast, addition of MC A4C resulted in a linear decay of the colloid fraction, which was 58.1 ± 1.7% 60 min after pH shift. Addition of HPMC 100LV stabilized the colloid fraction even more when, compared to MC A4C; the colloid fraction dropped to 95.4 ± 0.4% within the first 10 min after the pH shift and persisted for the remaining duration of the test. The influence of the other tested excipients on the colloid fraction profile is shown in Sup. 3 and Sup.4. The addition of HPMC 4M and HPMC 15LV showed a similar effect on the colloid fraction profile as the addition of HPMC 100LV given that the colloid fractions were stabilized at high levels within 10 min after the pH shift. Also, the combination of ALB with COP maintained the colloid fractions at high levels. A linear decay of the colloid fraction within the first 5 min after the pH shift was followed by a stabilization of the colloid fraction which was still 90.7 ± 2.0% 55 min later. The linear decay of the colloid fraction was observed for 10 min and 5 min in combination with the HPC grades and PVP grades, respectively. Following the decay phase, the colloid fractions were stabilized at constant levels that were lower than the levels resulting from the combination with the HPMC grades and COP. It was noticeable that PVP-K12 produced significantly lower colloid fractions than the other PVP grades as well as the HPC grades. The addition of both PEG grades did not affect the colloid fraction profile of separated ALB species. Similar to neat ALB, a high colloid fraction was observed only 1 min after the pH shift. Thereafter, the colloid fractions were consistently observed at extremely low levels.

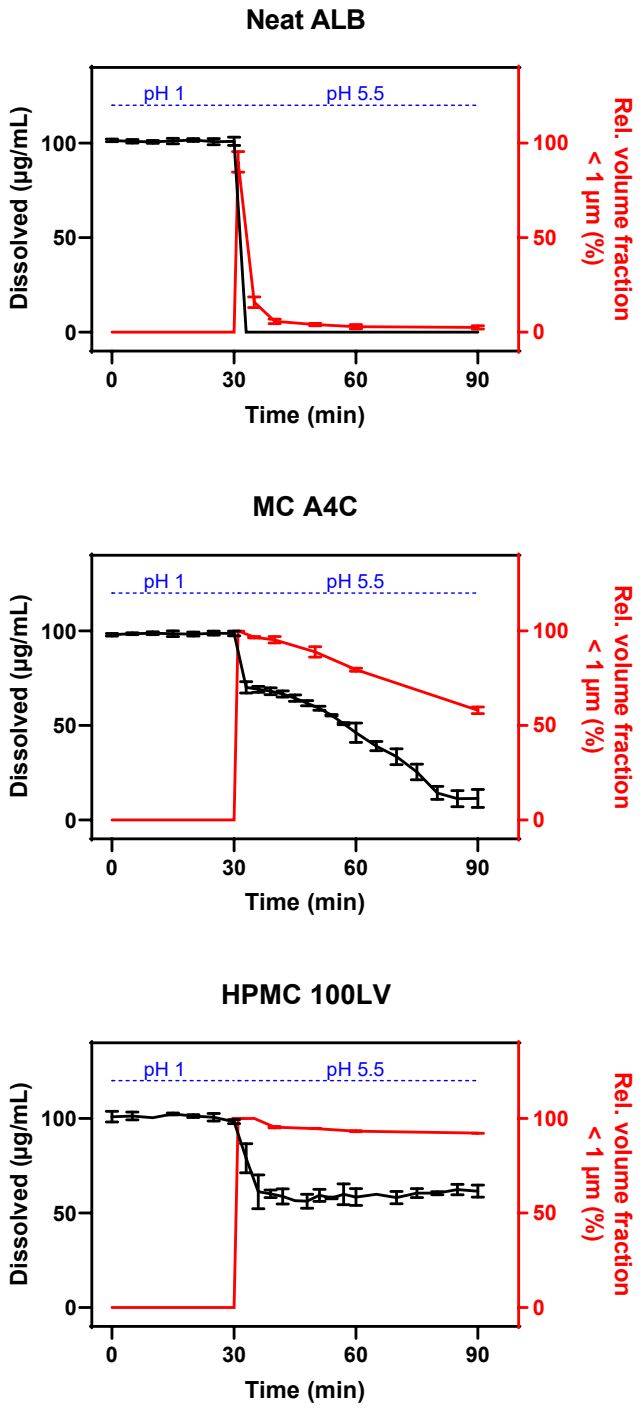

Fig. 4. Red lines show the kinetic colloid fraction profiles of ALB measured by laser diffraction. Colloid fraction profiles represent the time-dependent and pH-dependent evolution of the proportion of colloidal species in relation to coarse precipitates. Black lines show the supersaturation profiles of ALB obtained from the supersaturation assay. The profiles are shown for neat ALB, the combination of ALB with MC A4C and the combination of ALB with HPMC 100LV. Colloid fraction profiles and supersaturation profiles show similar trajectories. Error bars represent the standard deviations of the values. The experiments were conducted in triplicate.

3.5 Supersaturation profiles

The supersaturation of ALB was induced with a pH shift from pH 1 to pH 5.5 after 30 min. Fig. 4, Sup. 3 and Sup. 4 show the supersaturation profiles of ALB represented as black lines obtained from the supersaturation assay. In the first 30 min at pH 1.0 ALB was completely dissolved, regardless whether tested alone or in combination with the excipients. After the pH shift, neat ALB immediately precipitated to an undetectable level. The first measurement at pH 5.5 was always performed after 33 min. With the exception of the PEG grades, all investigated polymers enabled supersaturation of ALB. Resultant supersaturation profiles were characterized by two phases: a kinetically unstable phase and a kinetically stable phase. The concentration of ALB pre-dissolved together with MC A4C dropped continuously to 11.3 ± 4.3 µg/mL within 55 min after the pH shift. When HPMC 100LV was present in the test medium, the drug concentration dropped linearly to 60.2 ± 2.0 µg/mL 9 min after the pH shift and was still found to be at 61.6 ± 3.2 µg/mL 51 min later. The influence of all other excipients on the supersaturation profile of ALB is shown in Sup. 3 and Sup. 4. From the combination of ALB with HPMC 15LV and HPMC 4M similar supersaturation profiles resulted as from the combination of ALB with HPMC 100LV. HPMC 4M and HPMC 15LV stabilized ALB concentrations at high levels within the first 9 min after the pH shift. Addition of COP resulted in a linear decrease of ALB concentration to 65.5 ± 3.7 µg/mL within the first 6 min after the pH-shift followed by a stabilization of concentration levels. Also, in combination with HPC grades and PVP grades, ALB was supersaturated, initially in a short unstable manner followed by a constant type of supersaturation until the last measurement point. In presence of HPC SL and HPC SSL the drug concentrations decreased sharply to 25.9 ± 6.0 µg/mL and 27.6 ± 4.7 µg/mL, respectively, within 9 min after the pH shift. Subsequently, the supersaturation profiles were stabilized at constant levels, which were significantly lower than the levels resulting from the combinations of ALB with the HPMC grades as well as with COP. The lowest supersaturation extent was observed when PVP K-12 was added to the test medium. As in the example of neat ALB, a complete precipitation was observed when both PEG 6k and PEG 10k were added to the test medium.

3.6 Solid-state of the separated phase

The X-ray diffractograms of ALB isolated after the pH shift are shown in Fig 5. In the case of neat ALB, reflection peaks typical for ALB crystals were detected at 18.1°, 24.6° and 25.2° 2θ for all measurements; even for the first one 10 min after pH shift, which indicates a rapid crystallization of ALB. Similar behavior was observed for ALB that precipitated from the PEG 10k-containing solution. In combination with MC A4C and PVP K-12, the recrystallization of the separated phase took place much later as one reflection peak at 18.1° 2θ appeared in the measurements, earliest after 40 min. The reflection peaks were not detected at any time in combination with HPMC 100LV, COP and HPC SSL, indicating an amorphous nature of the separated drug phase for the entire test time of 60 min.

3.7 FF-EM imaging of the separated drug phase

Fig. 6, 7 and 8 show the freeze-fracture electron microscopy (FF-EM) images of the replicas that resulted from the ALB samples after the pH shift. Species smaller than 1 µm were detected in the investigated samples, including neat ALB as well as ALB in combination with MC A4C and HPMC 100LV, respectively. The replicas showed dark circular formations. The fact that the angular notches present in the formations could be caused by artifacts during freeze-fracture preparation cannot be exclusively ruled out. Hence, this effect should be ignored at this juncture. The formations appeared flat, which implies that the structures were cut through instead of fractured. Incomplete removal might have induced electron micrographic contrast by the sample material itself instead of the shadowing platinum film. Irrespective of the origin of electron contrast, it permits the estimation of the formation diameters.

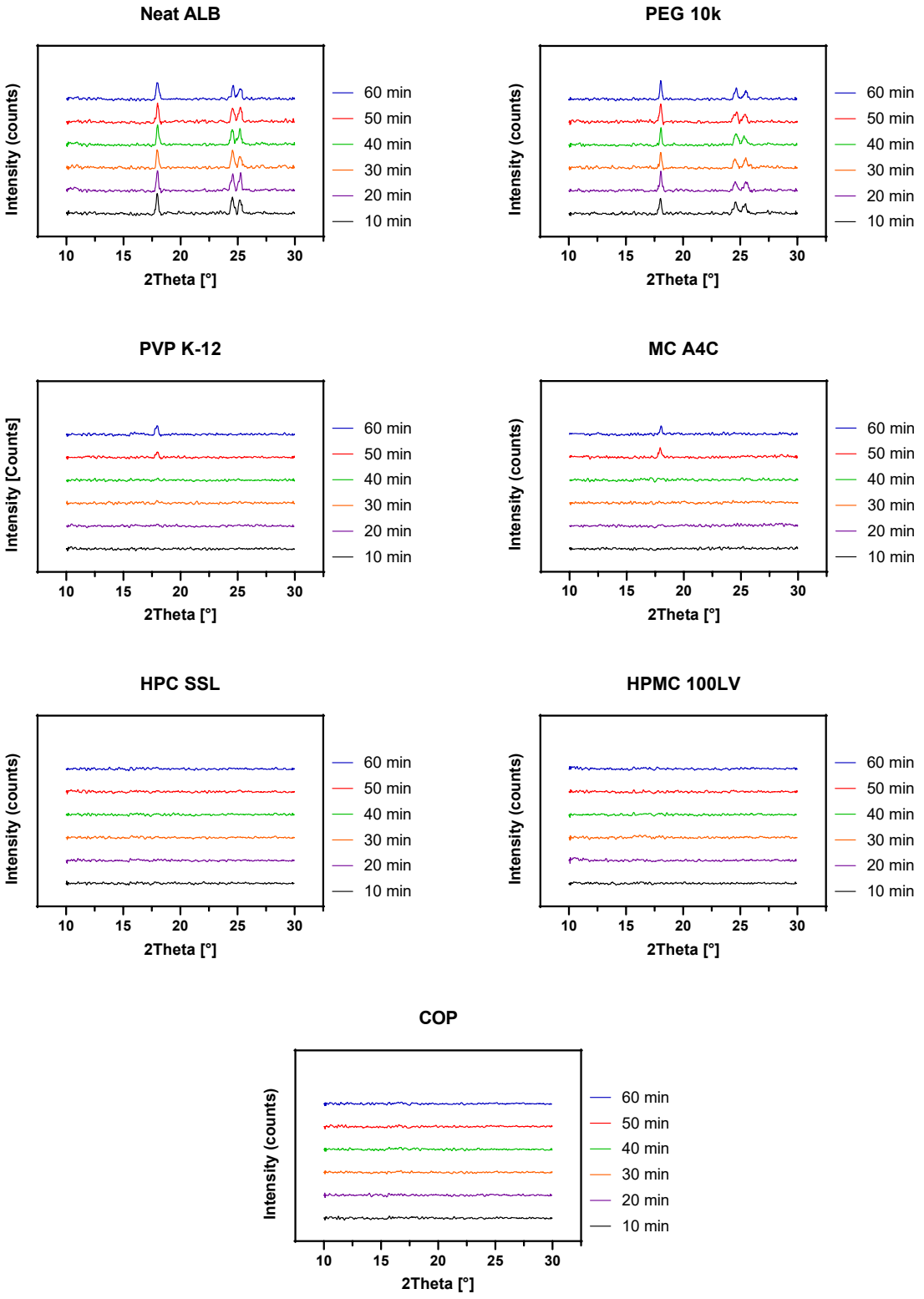

Fig. 5. Time-dependent solid-state of ALB isolated in presence and absence of various excipients after the shift from pH 1 to pH 5.5. Samples were analyzed by means of transmission X-ray diffraction (XRD). Each sample was measured six times in succession.

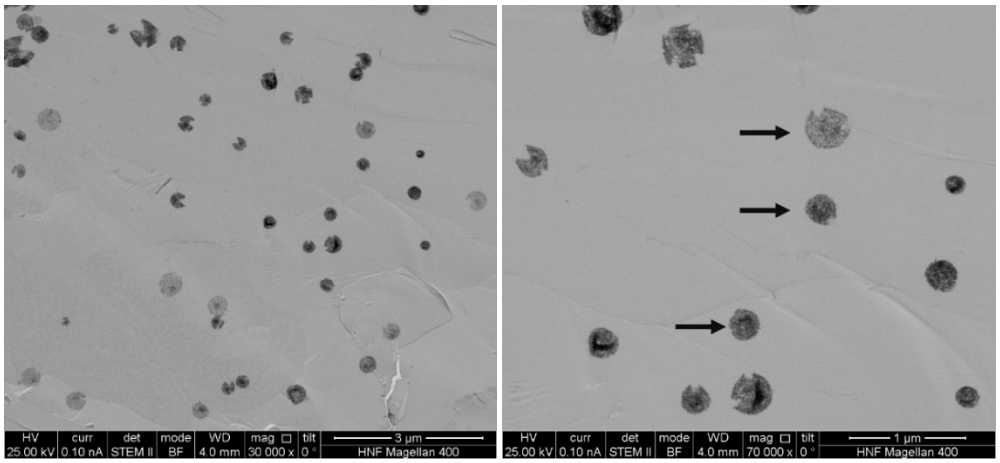

Fig. 6. ALB species formed after the shift from pH 1 to pH 5.5. All figures are transmission electron micrographs of shadow-cast replicas; direction of shadow is bottom to top, arrows in the right-hand image highlighting circular formations interpreted as albendazole aggregates.

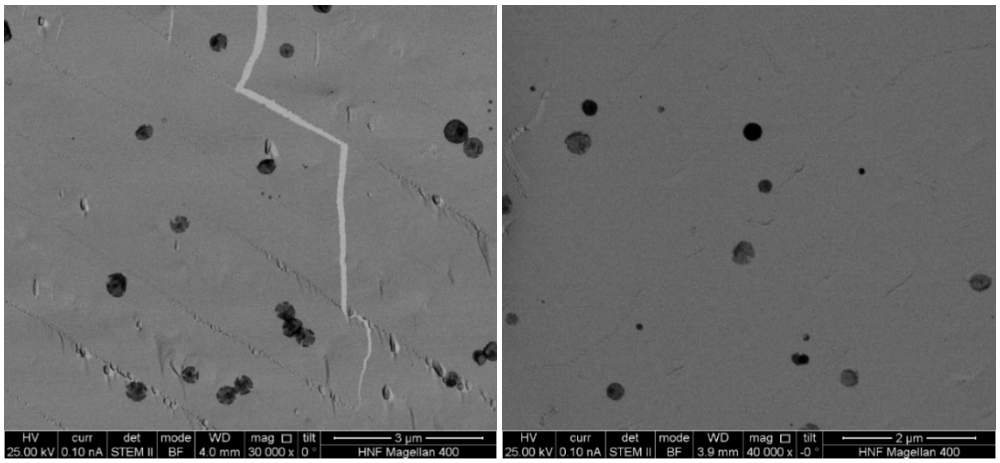

Fig. 7. ALB species formed in presence of MC A4C after the shift from pH 1 to pH 5.5. All figures are transmission electron micrographs of shadow-cast replicas; direction of shadow is bottom to top.

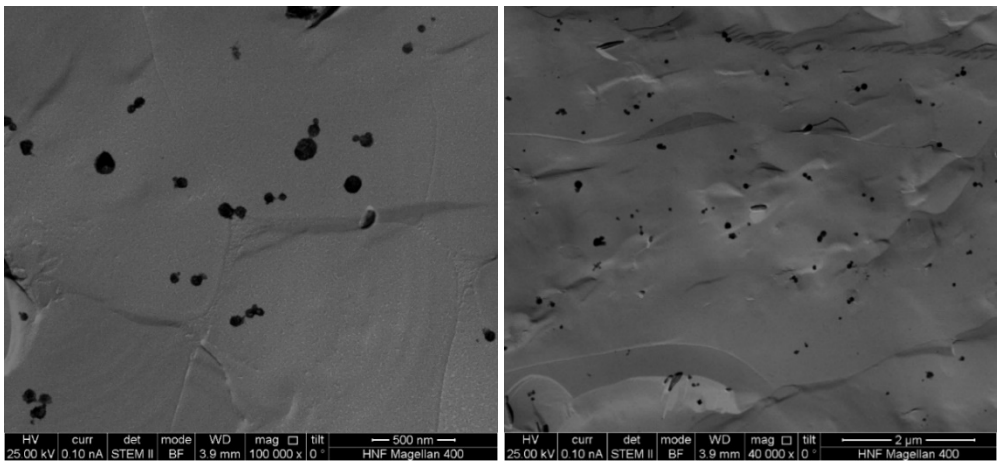

Fig. 8. ALB species formed in presence of HPMC 100LV after the shift from pH 1 to pH 5.5. All figures are transmission electron micrographs of shadow-cast replicas; direction of shadow is bottom to top.

4 Discussion

Both phenomena of supersaturation and precipitation were induced by the pH-shift, as the saturation solubility of ALB decreased strongly at pH 5.5 due to a conversion of the protonated molecule to the free base (Fig. 1). As a consequence, the free ALB base rapidly separated from the solution in the form of amorphous nano-sized species that created a second phase, the separated amorphous colloidal phase. Albeit such phase separation phenomena are frequently referred to as liquid-liquid phase separation, their accordance to the definition of Ilevbare and Taylor (2013) is still speculative. However, the formation of these separated amorphous colloidal phase was of utmost importance. The proposed phase separation and precipitation behavior induced by a pH shift in dependence of polymers is shown in Fig. 9. Remarkably, the stabilization of the nano-sized species depended strongly on the ALB-polymer combinations. Furthermore, the ability of polymers to stabilize the separated phase in terms of size and solid-state correlated with their ability to stabilize supersaturation. Subsequently, a dependence between the extent of supersaturation and the extent of amorphous colloidal phase separation was found and consequently an increase in the AUCs of the colloid fraction profiles led to an increase in the AUCs of the supersaturation profiles (Fig. 10). In Fig. 10, a simple linear regression yielded a r^2 of 0.8537. Briefly, polymers that enabled supersaturation stabilized the separated amorphous colloid fraction over time. In contrast, polymers as well as the neat drug, which did not allow for supersaturation, failed to stabilize the amorphous colloid fraction over time resulting in fast recrystallization and the growth of the separated drug species. In other words, polymer-stabilized colloids prevent on one hand the precipitation of the drug as amorphous or crystalline solids, and on the other hand, act as a hub for supersaturated drug molecules. Interestingly, the size of the colloids measured by DLS did not strongly impact the supersaturation as long as they remained below 1 µm. It should be considered that the potential sedimentation of large precipitates might affect the Brownian motion, thus limiting the accuracy of DLS analyses. However, the introduced method for characterization of phase separation behavior based on at-line LD could represent an attempt to overcome limitations of DLS analyses. Unlike DLS analyses, which are widely applied for phase separation characterization of small drug molecules, LD enabled a simultaneous detection of both large precipitates (> 1 µm) and nano-sized colloids (< 1 µm).

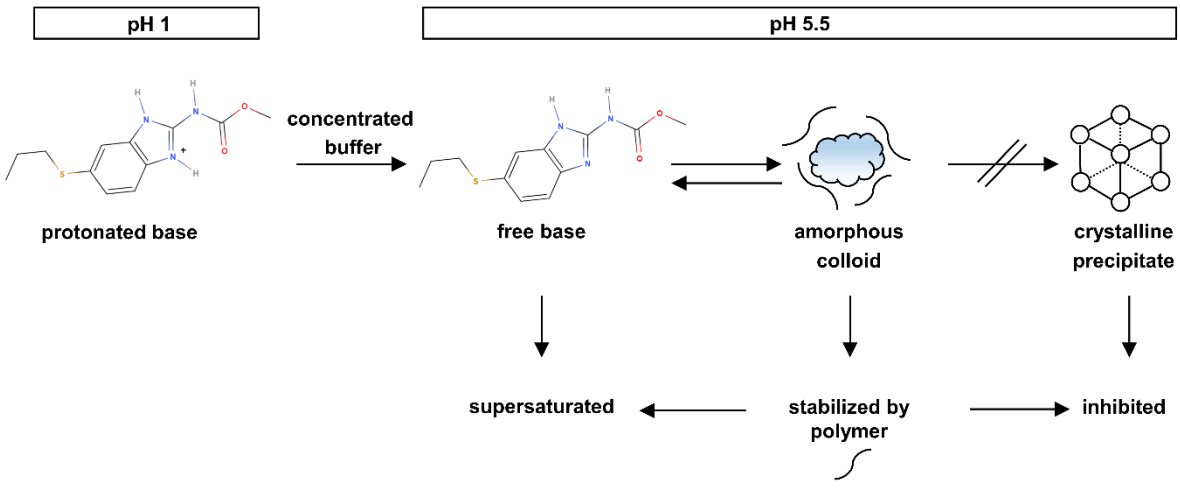

Fig. 9. Schematic of the proposed phase separation behavior of ALB in dependence of pH and polymer combination. The free ALB base was supersaturated as the amorphous drug colloids were stabilized by polymers, which in turn inhibited recrystallization.

The supersaturation profiles and the colloidal fraction profiles were characterized by two sequences, namely a short kinetically unstable period followed by a kinetically stable period. The time to stabilize supersaturation corresponded to the time needed to stabilize the colloid fraction. Consequently, the trajectory of the supersaturation profiles correlated with the trajectory of the colloid fraction profiles, strongly suggesting a fixed ratio between supersaturation and colloid fraction. A proposed mechanism for the dependence of supersaturation on the stabilization of the colloid fraction might be related to the creation of a microenvironment around the separated colloids recognized as soft matter phenomenon, where the dissolved drug molecules are in balance with the aforementioned colloids. This is supported by recent findings that dissolved drug molecules have a reduced mobility on the surface of the separated colloids (Ueda et al., 2019). Furthermore, a molecular exchange between the dissolved drug and the separated colloids might take place (Ueda et al., 2019). The polymer-induced stabilization of the colloid fraction in aqueous media is presumably based on the assumption that dissolved polymers adsorb to the often partially apolar surfaces of colloidal particles due to surface interactions resulting in steric hindrances, which prevent both aggregation and coalescence of the colloids dependent on the drug polymer combination (Ganesh et al., 2018, 2017; Indulkar et al., 2016; Shen et al., 2016; Ueda et al., 2019).

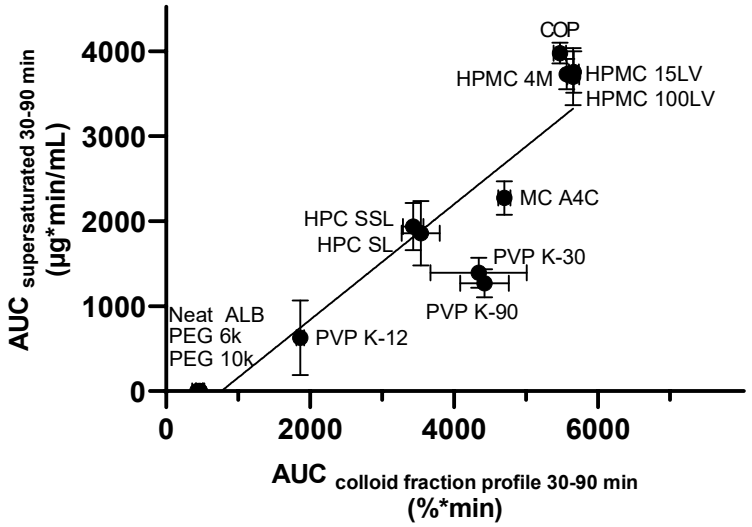

Fig. 10. Correlation between extent of supersaturation and extent of amorphous colloidal phase separation. The area under the curve (AUC) of the colloid fraction profiles and the supersaturation profiles were plotted against each other. The higher the extent of amorphous colloidal phase separation the more ALB molecules were supersaturated.

5 Conclusion

In case of the BCS Class II model drug albendazole (ALB) pH-dependent supersaturation was governed by a phase separation, which was identified as an amorphous colloidal phase separation similarly observed upon supersaturation of several other drugs (França et al., 2020; Muschol and Rosenberger, 1997; Ueda et al., 2019). The concept of phase separation involved in drug supersaturation was supported for the first time by visualization of the nano-sized species via freeze-fracture electron microscopy (FF-EM). The nature of the of drug-polymer combinations not only determined the extent of the rapid transformation of the amorphous colloidal phase to crystalline precipitates, but also

influenced the extent of supersaturation as well as the associated kinetics. In this study, the introduced approach to determine the relationship between the amorphous colloidal phase separation and supersaturation involved an at-line size monitoring combined with time-dependent solid-state monitoring of colloids and precipitates resulting in a relative quantification of the nano-sized drug species, described as colloid fraction. As a consequence, a kinetic profile of the colloid fraction could be established. For all investigated twelve polymers these kinetic profiles built the foundation of a correlation between the extent of amorphous colloidal phase separation and extent of supersaturation. From these findings a fixed ratio between supersaturated drug molecules and the separated amorphous colloidal drug phase, the so-called colloid fraction was concluded. Moreover, it supports the concept that a phase-separated colloidal drug phase serves as a reservoir for dissolved drug molecules confirming the hypothesis of various authors (Indulkar et al., 2016; Raina et al., 2014; Taylor and Zhang, 2016). While recent studies emphasized the significance of the colloid size on supersaturation of poorly water-soluble drugs (França et al., 2020; Ueda et al., 2019) our studies suggest that the proportion of them in dependence of the precipitate should be considered as an additional key factor determining supersaturation performance and kinetics as long as their amorphous and colloidal nature is stabilized. Furthermore, these studies demonstrated the high significance of separated amorphous drug colloids for supersaturation kinetics in addition to the reported intermolecular interactions between polymers and drug molecules in the dissolved state (Anwar et al., 2009; Chen et al., 2019). In conclusion, the dependence of supersaturation on amorphous colloidal phase separation was clarified, allowing for an optimized and simple assessment of supersaturating drug delivery systems (e.g. of amorphous solid dispersion) designed to enhance bioavailability of poorly water-soluble drugs, as the dissolved molecules are absorbed *in vivo* (Wilson et al., 2018). Ongoing studies are seeking to determine the impact of polymeric surfactants on the interplay of colloid fractions and supersaturation, as they might stabilize colloidal soft matter very efficiently due to their highly surface active groups.

6 Acknowledgement

We would like to acknowledge language editing and proofreading by Maryam Shetab Boushehri and Henusha Jhundoo.

7 References

Albrecht, W., Moers, J., Hermanns, B., 2017. HNF - Helmholtz Nano Facility. Journal of large-scale research facilities JLSRF 3, 112. https://doi.org/10.17815/jlsrf-3-158

Amidon, G.L., Lennernäs, H., Shah, V.P., Crison, J.R., 1995. A theoretical basis for a biopharmaceutic drug classification: the correlation of in vitro drug product dissolution and in vivo bioavailability. Pharm. Res. 12, 413–420.

Anwar, J., Boateng, P.K., Tamaki, R., Odedra, S., 2009. Mode of Action and Design Rules for Additives That Modulate Crystal Nucleation. Angewandte Chemie International Edition 48, 1596–1600. https://doi.org/10.1002/anie.200804553

Chen, Y., Pui, Y., Chen, H., Wang, S., Serno, P., Tonnis, W., Chen, L., Qian, F., 2019. Polymer-Mediated Drug Supersaturation Controlled by Drug–Polymer Interactions Persisting in an Aqueous Environment. Mol. Pharmaceutics 16, 205–213. https://doi.org/10.1021/acs.molpharmaceut.8b00947

Fong, S.Y.K., Bauer-Brandl, A., Brandl, M., 2017. Oral bioavailability enhancement through supersaturation: an update and meta-analysis. Expert Opinion on Drug Delivery 14, 403–426. https://doi.org/10.1080/17425247.2016.1218465

França, M.T., Martins Marcos, T., A. Costa, P.F., P. Gerola, A., Stulzer, H.K., 2020. The role of glycyrrhizic acid in colloidal phenomena of supersaturation drug delivery systems containing the antifungal drug griseofulvin. Journal of Molecular Liquids 301, 112336. https://doi.org/10.1016/j.molliq.2019.112336

Ganesh, A.N., Donders, E.N., Shoichet, B.K., Shoichet, M.S., 2018. Colloidal aggregation: From screening nuisance to formulation nuance. Nano Today 19, 188–200. https://doi.org/10.1016/j.nantod.2018.02.011

Ganesh, A.N., Logie, J., McLaughlin, C.K., Barthel, B.L., Koch, T.H., Shoichet, B.K., Shoichet, M.S., 2017. Leveraging Colloidal Aggregation for Drug-Rich Nanoparticle Formulations. Mol. Pharmaceutics 14, 1852–1860. https://doi.org/10.1021/acs.molpharmaceut.6b01015

Guzmán, H.R., Tawa, M., Zhang, Z., Ratanabanangkoon, P., Shaw, P., Gardner, C.R., Chen, H., Moreau, J.-P., Almarsson, Ö., Remenar, J.F., 2007. Combined use of crystalline salt forms and precipitation inhibitors to improve oral absorption of celecoxib from solid oral formulations. Journal of Pharmaceutical Sciences 96, 2686–2702. https://doi.org/10.1002/jps.20906

Ilevbare, G.A., Taylor, L.S., 2013. Liquid–Liquid Phase Separation in Highly Supersaturated Aqueous Solutions of Poorly Water-Soluble Drugs: Implications for Solubility Enhancing Formulations. Crystal Growth & Design 13, 1497–1509. https://doi.org/10.1021/cg301679h

Indulkar, A.S., Box, K.J., Taylor, R., Ruiz, R., Taylor, L.S., 2015. pH-Dependent Liquid–Liquid Phase Separation of Highly Supersaturated Solutions of Weakly Basic Drugs. Mol. Pharmaceutics 12, 2365–2377. https://doi.org/10.1021/acs.molpharmaceut.5b00056

Indulkar, A.S., Gao, Y., Raina, S.A., Zhang, G.G.Z., Taylor, L.S., 2016. Exploiting the Phenomenon of Liquid–Liquid Phase Separation for Enhanced and Sustained Membrane Transport of a Poorly Water-Soluble Drug. Mol. Pharmaceutics 13, 2059–2069. https://doi.org/10.1021/acs.molpharmaceut.6b00202

Kawakami, K., 2017. Supersaturation and crystallization: non-equilibrium dynamics of amorphous solid dispersions for oral drug delivery. Expert Opinion on Drug Delivery 14, 735–743. https://doi.org/10.1080/17425247.2017.1230099

Kesisoglou, F., Wang, M., Galipeau, K., Harmon, P., Okoh, G., Xu, W., 2019. Effect of Amorphous Nanoparticle Size on Bioavailability of Anacetrapib in Dogs. J Pharm Sci 108, 2917–2925. https://doi.org/10.1016/j.xphs.2019.04.006

Kohri, N., Yamayoshi, Y., Xin, H., Iseki, K., Sato, N., Todo, S., Miyazaki, K., 1999. Improving the Oral Bioavailability of Albendazole in Rabbits by the Solid Dispersion Technique. Journal of Pharmacy and Pharmacology 51, 159–164. https://doi.org/10.1211/0022357991772277

Laitinen, R., Löbmann, K., Grohganz, H., Priemel, P., Strachan, C.J., Rades, T., 2017. Supersaturating drug delivery systems: The potential of co-amorphous drug formulations. International Journal of Pharmaceutics 532, 1–12. https://doi.org/10.1016/j.ijpharm.2017.08.123

Monschke, M., Wagner, K.G., 2019. Amorphous solid dispersions of weak bases with pH-dependent soluble polymers to overcome limited bioavailability due to gastric pH variability – An in-vitro approach. International Journal of Pharmaceutics 564, 162–170. https://doi.org/10.1016/j.ijpharm.2019.04.034

Moor, H., Mühlethaler, K., 1963. Fine Structure in Frozen-Etched Yeast Cells. J Cell Biol 17, 609–628.

Morrison, J., Nophsker, M., Elzinga, P., Donoso, M., Park, H., Haskell, R., 2017. A polychromatic turbidity microplate assay to distinguish discovery stage drug molecules with beneficial precipitation properties. International Journal of Pharmaceutics 531, 24–34. https://doi.org/10.1016/j.ijpharm.2017.07.086

Muschol, M., Rosenberger, F., 1997. Liquid–liquid phase separation in supersaturated lysozyme solutions and associated precipitate formation/crystallization. J. Chem. Phys. 107, 1953–1962. https://doi.org/10.1063/1.474547

Raina, S.A., Van Eerdenbrugh, B., Alonzo, D.E., Mo, H., Zhang, G.G.Z., Gao, Y., Taylor, L.S., 2015. Trends in the precipitation and crystallization behavior of supersaturated aqueous solutions of poorly water-soluble drugs assessed using synchrotron radiation. J Pharm Sci 104, 1981–1992. https://doi.org/10.1002/jps.24423

Raina, S.A., Zhang, G.G.Z., Alonzo, D.E., Wu, J., Zhu, D., Catron, N.D., Gao, Y., Taylor, L.S., 2014. Enhancements and Limits in Drug Membrane Transport Using Supersaturated Solutions of Poorly Water Soluble Drugs. Journal of Pharmaceutical Sciences 103, 2736–2748. https://doi.org/10.1002/jps.23826

Severs, N.J., 2007. Freeze-fracture electron microscopy. Nature Protocols 2, 547–576. https://doi.org/10.1038/nprot.2007.55

Shen, G., Xing, R., Zhang, N., Chen, C., Ma, G., Yan, X., 2016. Interfacial Cohesion and Assembly of Bioadhesive Molecules for Design of Long-Term Stable Hydrophobic Nanodrugs toward Effective Anticancer Therapy. ACS Nano 10, 5720–5729. https://doi.org/10.1021/acsnano.5b07276

Stewart, A.M., Grass, M.E., Brodeur, T.J., Goodwin, A.K., Morgen, M.M., Friesen, D.T., Vodak, D.T., 2017. Impact of Drug-Rich Colloids of Itraconazole and HPMCAS on Membrane Flux in Vitro and Oral Bioavailability in Rats. Mol. Pharmaceutics 14, 2437–2449. https://doi.org/10.1021/acs.molpharmaceut.7b00338

Surasarang, S.H., Keen, J.M., Huang, S., Zhang, F., McGinity, J.W., III, R.O.W., 2017. Hot melt extrusion versus spray drying: hot melt extrusion degrades albendazole. Drug Development and Industrial Pharmacy 43, 797–811. https://doi.org/10.1080/03639045.2016.1220577

Taylor, L.S., Zhang, G.G.Z., 2016. Physical chemistry of supersaturated solutions and implications for oral absorption. Advanced Drug Delivery Reviews, Understanding the challenges of beyond-rule-of-5 compounds 101, 122–142. https://doi.org/10.1016/j.addr.2016.03.006

Ueda, K., Higashi, K., Moribe, K., 2019. Mechanistic elucidation of formation of drug-rich amorphous nanodroplets by dissolution of the solid dispersion formulation. Int J Pharm 561, 82–92. https://doi.org/10.1016/j.ijpharm.2019.02.034

Van Eerdenbrugh, B., Raina, S., Hsieh, Y.-L., Augustijns, P., Taylor, L.S., 2014. Classification of the crystallization behavior of amorphous active pharmaceutical ingredients in aqueous environments. Pharm Res 31, 969–982. https://doi.org/10.1007/s11095-013-1216-z

Wilson, V., Lou, X., Osterling, D.J., Stolarik, D.F., Jenkins, G., Gao, W., Zhang, G.G.Z., Taylor, L.S., 2018. Relationship between amorphous solid dispersion in vivo absorption and in vitro dissolution: phase behavior during dissolution, speciation, and membrane mass transport. J Control Release 292, 172–182. https://doi.org/10.1016/j.jconrel.2018.11.003

Zecevic, D.E., Wagner, K.G., 2013. Rational Development of Solid Dispersions via Hot-Melt Extrusion Using Screening, Material Characterization, and Numeric Simulation Tools. Journal of Pharmaceutical Sciences 102, 2297–2310. https://doi.org/10.1002/jps.23592

Supplementary data

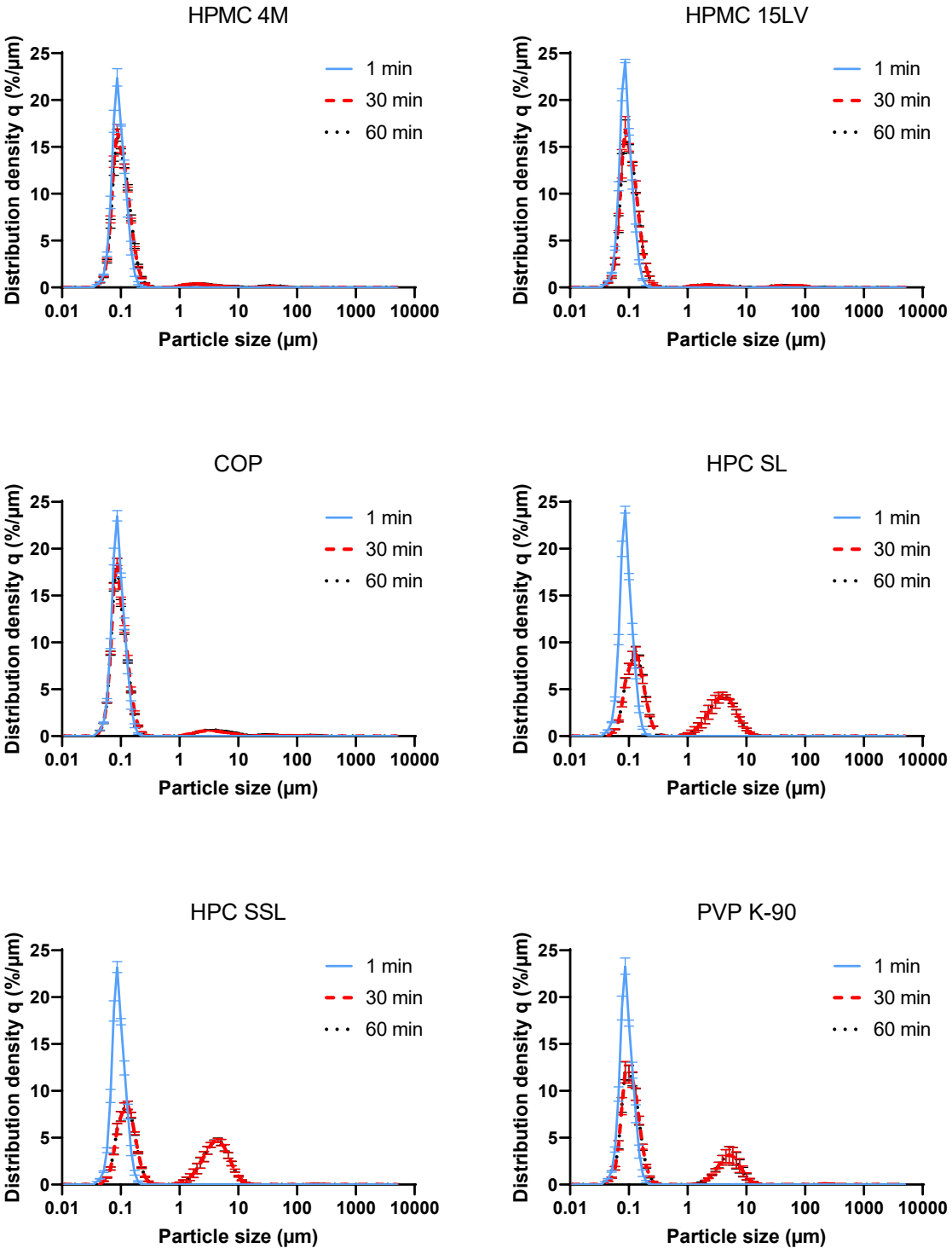

Sup. 1. Volume-based particle size distributions of ALB species measured by means of laser diffraction in presence of various polymers. The blue solid line, the red dashed line and the black dotted line were obtained 1 min, 30 min and 60 min the shift from pH 1 to pH 5.5, respectively. Bimodal distributions indicate that a colloid fraction and a coarse fraction were formed after the pH shift. Peak heights changed over time depending on the type of the polymer added. Error bars represent the standard deviations of the values. The experiments were conducted in triplicate.

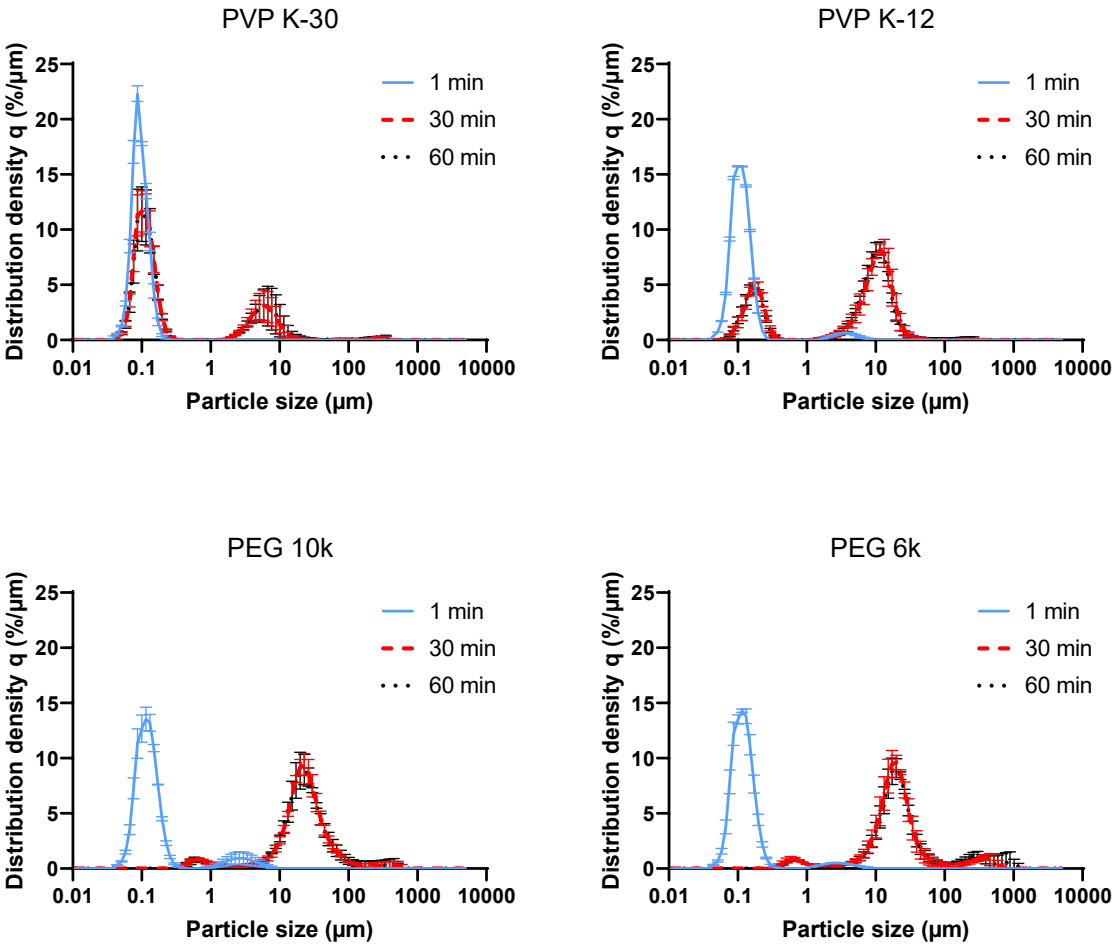

Sup. 2. Volume-based particle size distributions of ALB species measured by means of laser diffraction in presence of various polymers. The blue solid line, the red dashed line and the black dotted line were obtained 1 min, 30 min and 60 min after the shift from pH 1 to pH 5.5, respectively. Bimodal distributions indicate that a colloid fraction and a coarse fraction were formed after the pH shift. Peak heights changed over time depending on the type of the polymer added. Error bars represent the standard deviations of the values. The experiments were conducted in triplicate.

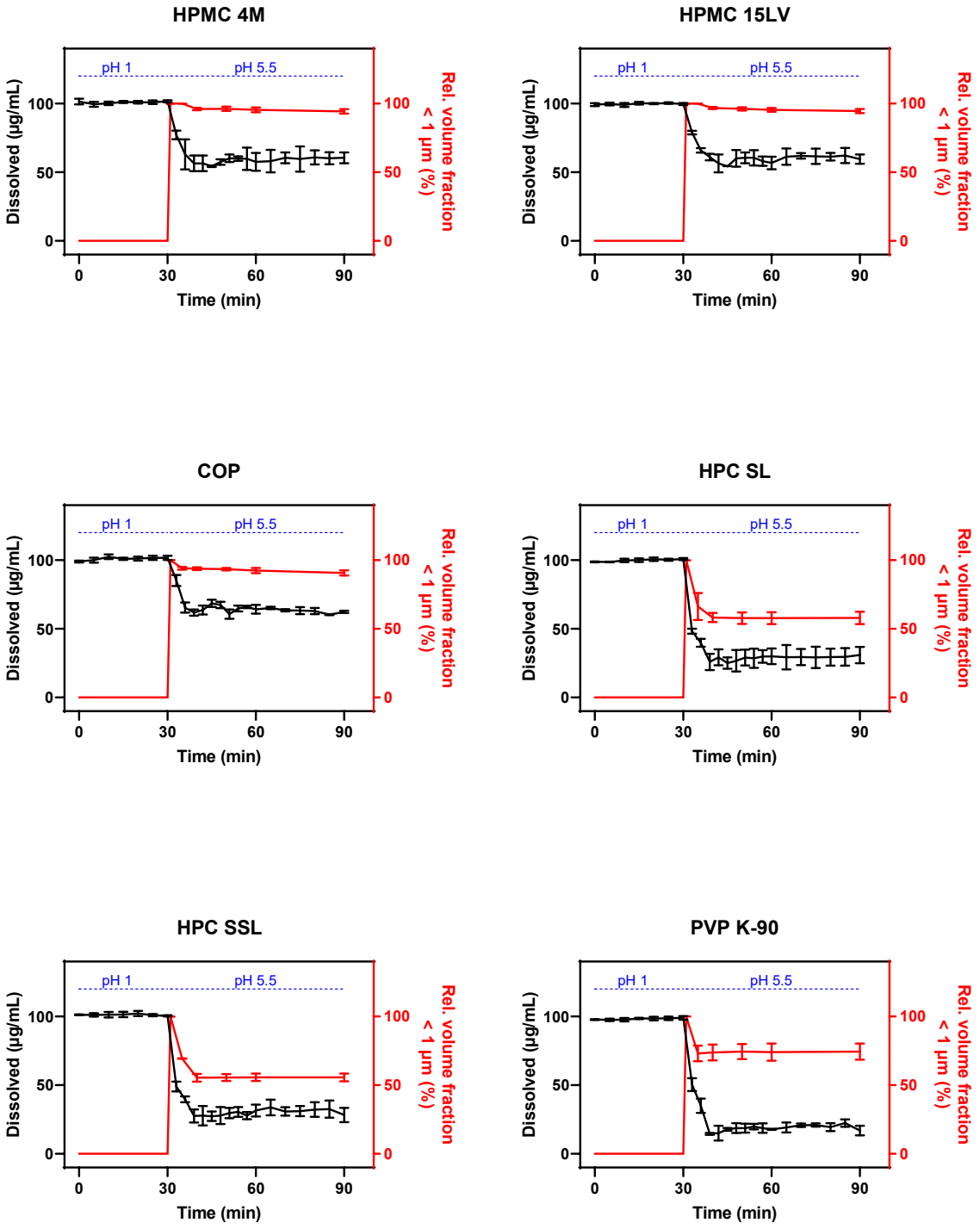

565

Sup. 3. Red lines show the kinetic colloid fraction profiles of ALB measured by laser diffraction. Colloid fraction profiles represent the time-dependent and pH-dependent evolution of the proportion of colloidal species in relation to coarse precipitates. Black lines show the supersaturation profiles of ALB obtained from the supersaturation assay. The profiles are shown for the combination of ALB with
570 various polymers. Colloid fraction profiles and supersaturation profiles show similar trajectories. Error bars represent the standard deviations of the values (n = 3). Error bars represent the standard deviations of the values. The experiments were conducted in triplicate.

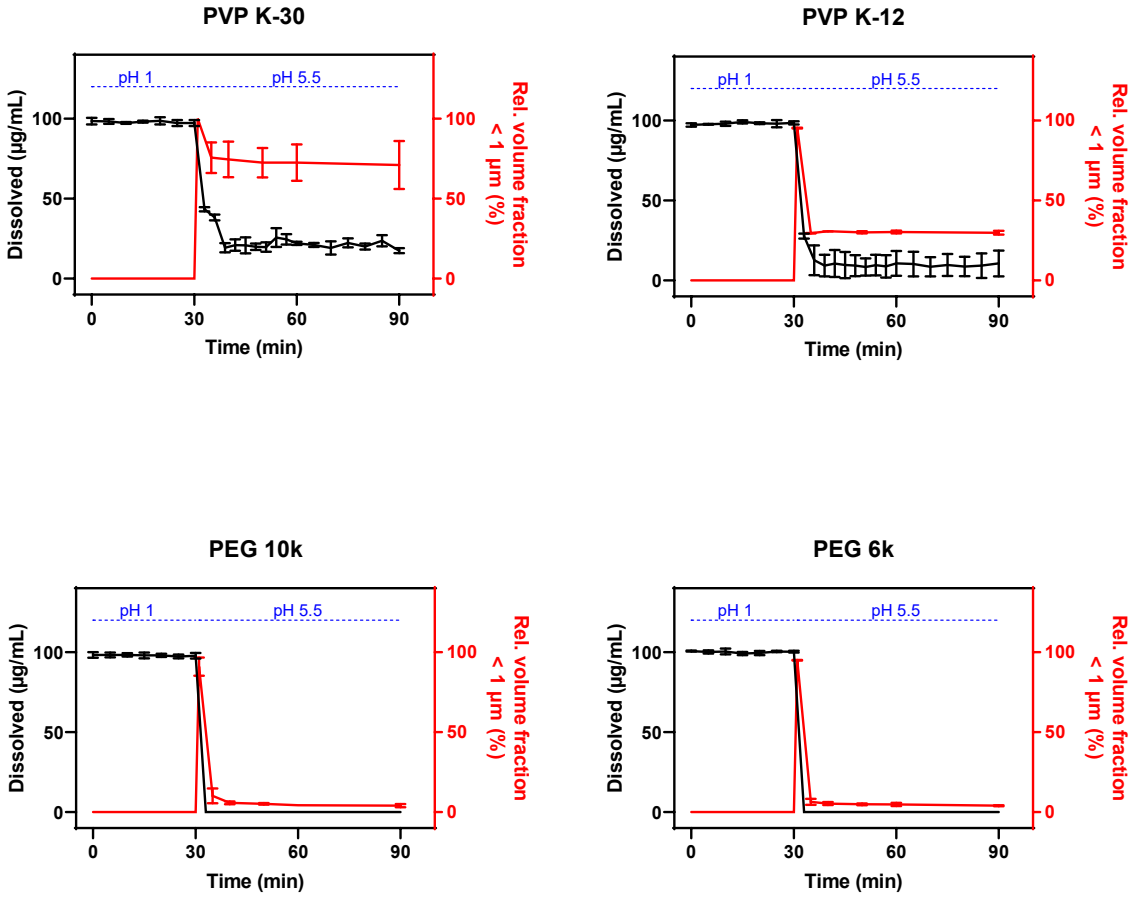

Sup. 4. Red lines show the kinetic colloid fraction profiles of albendazole (ALB) measured by laser diffraction. Colloid fraction profiles represent the time-dependent and pH-dependent evolution of the proportion of colloidal species in relation to coarse precipitates. Black lines show the supersaturation profiles of ALB obtained from the supersaturation assay. The profiles are shown for the combination of ALB with various polymers. Colloid fraction profiles and supersaturation profiles show similar trajectories. Error bars represent the standard deviations of the values. The experiments were conducted in triplicate.

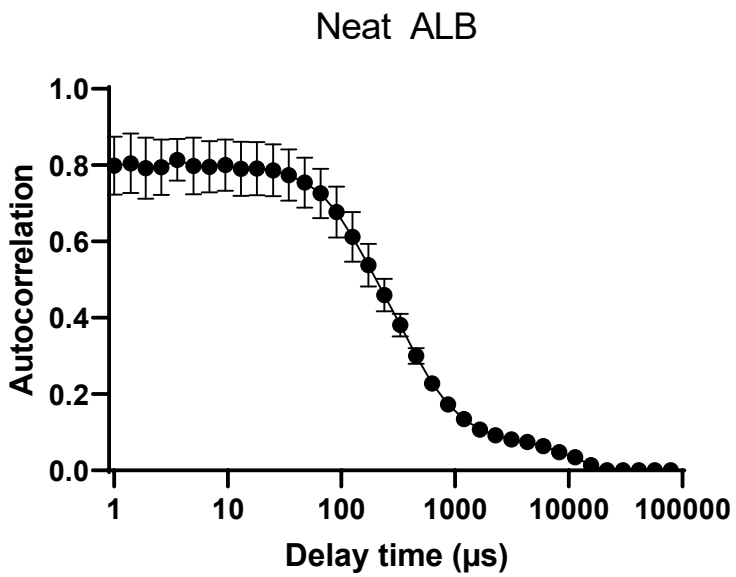

Sup. 5. Autocorrelation function derived from dynamic light scattering (DLS) measurements of neat ALB at pH 5.5. Presence of large particles is indicated by long lasting autocorrelation (1000 µs – 10000 µs). Error bars represent the standard deviations of the values. The experiments were conducted in triplicate.